MICHIGAN STATE
UNIVERSITY

National Superconducting Cyclotron Laboratory

PROTON SCATTERING BY THE UNSTABLE NEUTRON-RICH ISOTOPES ^{42,44}Ar

H. SCHEIT, F. MARÉCHAL, T. GLASMACHER, E. BAUGE, Y. BLUMENFELD, J.P. DELAROCHE, J. LIBERT, M. GIROD, R.W. IBBOTSON, K.W. KEMPER, B. PRITYCHENKO, and T. SUOMIJÄRVI

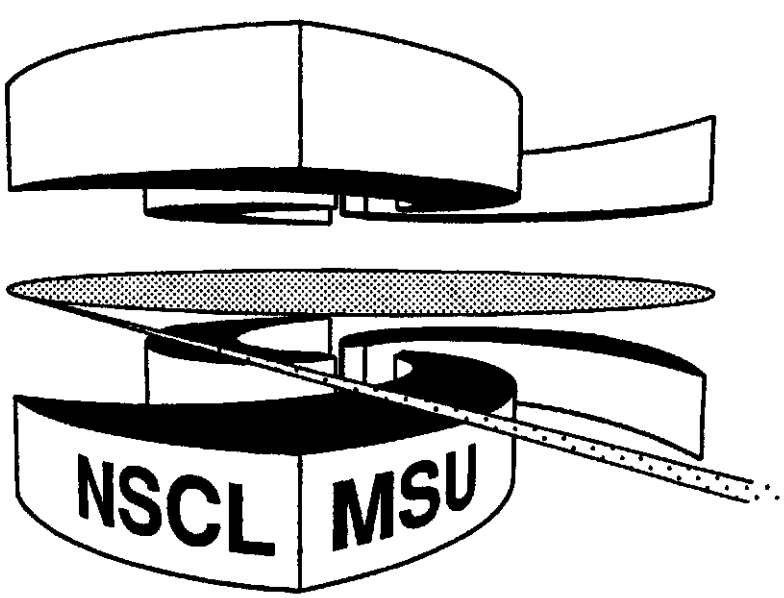

MSUCL-1162 **JUNE 2000**

Proton scattering by the unstable neutron-rich isotopes ^{42,44}Ar

H. Scheit,[1,2,*] F. Maréchal,[3] T. Glasmacher,[1,2] E. Bauge,[4] Y. Blumenfeld,[5] J.P. Delaroche,[4] J. Libert,[5] M. Girod,[4] R.W. Ibbotson,[3] K.W. Kemper,[3] B. Pritychenko,[1,2] and T. Suomijärvi[5]

[1] National Superconducting Cyclotron Laboratory, Michigan State University, East Lansing, Michigan 48824

[2] Department of Physics and Astronomy, Michigan State University, East Lansing, Michigan 48824

[3] Department of Physics, Florida State University, Tallahassee, Florida 32306

[4] Commissariat à l'Energie Atomique, Service de Physique Nucléaire, Boîte Postale 12, 91680 Bruyères-le-Châtel, France

[5] Institut de Physique Nucléaire, IN$_2$P$_3$-CNRS, 91406 Orsay, France

(June 13, 2000)

Abstract

Elastic and inelastic proton scattering to the 2_1^+ states of the neutron-rich argon isotopes ^{42}Ar and ^{44}Ar have been measured in inverse kinematics with a beam energy of 33 MeV/nucleon. Phenomenological distorted wave Born approximation calculations are compared with the data and quadrupole deformation parameters of $\beta_2 = 0.32 \pm 0.05$ and $\beta_2 = 0.31 \pm 0.05$ are extracted for the 2_1^+ states in ^{42}Ar and ^{44}Ar, respectively. A consistent microscopic proton scattering analysis has been applied to all even-even argon isotopes from $A=36$ to $A=44$. This analysis used microscopic collective model densities and a modiied Jeukenne-Lejeune-Mahaux nucleon-nucleon effective interaction. The predicted cross sections agree very well with the experimental data, making this microscopic analysis a powerful tool to teat the structure of nuclei

far from stability.

PACS numbers: 21.10.Re, 25.40.Cm, 25.40.Ep, 25.60.Bx

I. INTRODUCTION

Excitation energies and $B(E2)$ values of the first 2^+ states in neutron-rich even-even Si, S and Ar isotopes in the mass $A = 40$ region have been recently measured by intermediate-energy Coulomb excitation [1–3]. These measurements revealed a rapid weakening of the $N = 28$ shell closure below ^{48}Ca and a region of moderate deformation around ^{40}S and ^{42}S, confirming the deformation effects calculated for the $N \approx 28$ isotones in this mass region and the erosion of the $N = 28$ shell gap due to the large neutron excess [4–6]. Proton scattering experiments on ^{38}S and ^{40}S added further evidence of this deformation region between the major $N = 20$ and $N = 28$ shell closures [7,8]. Proton scattering results are complementary to those obtained by Coulomb excitation because the electromagnetic excitation probes the protons in the nucleus, while proton scattering at energies around 30 MeV, is mainly sensitive to the neutrons [9]. Numerous proton inelastic scattering experiments using unstable beams have been reported [7,8,10–14], providing information on nuclear structure and interaction potentials outside the valley of stability, where isospin effects are expected to be important.

The question arises as to how the nuclear structure and the neutron and proton matter distributions of these exotic nuclei evolve far from stability. Extracting nuclear properties, such as density distributions, from proton scattering relies on interaction models, the parameters of which are adjusted to reproduce the experimental results. Microscopic approaches, where nuclear densities are folded with an effective nucleon-nucleon interaction to produce the optical model potentials, are commonly used to study the nuclear structure of stable and unstable nuclei. Once the parameters of the effective interaction are fixed, the analysis is then sensitive to the nuclear density distributions. Very recently, such a microscopic single-scattering-model study of elastic and inelastic proton scattering from even-even sulfur isotopes has been reported for beam energies around 30 MeV/nucleon [8]. In the sulfur case, the results suggest the presence of a neutron skin in the most neutron-rich isotopes. In other studies, neutron densities and radial shapes of transition densities to several levels, including the first and second 2^+ states, have been experimentally unfolded for nuclei such as ^{32}S [15],

^{34}S [16] and ^{48}Ca [17], using the proton densities determined from electron scattering.

The present work reports the results of a study of the neutron-rich argon isotopes through proton scattering in inverse kinematics. Excitation energy spectra and angular distributions were obtained through the measurement of the energies and angles of recoiling protons over a broad angular range with a silicon-strip detector array. Quadrupole deformation parameters were extracted for the 2_1^+ states in these two nuclei using distorted wave Born approximation calculations and standard Wood-Saxon phenomenological optical potentials. A complete analysis using microscopic collective model densities folded with a modified Jeukenne-Lejeune-Mahaux (JLM) nucleon-nucleon effective interaction is also presented for all even-even argon isotopes from $A=36$ to $A=44$.

The paper is organized as follows. Section II is devoted to the experimental procedure and results. Section III presents the phenomenological analysis of the data as well as the description and discussion of the microscopic analysis performed for the argon isotopic chain. Finally, the findings are summarized and conclusions are drawn in Sec. IV.

II. EXPERIMENT

The secondary ^{42,44}Ar beams were produced via fragmentation of a 70 MeV/nucleon ^{48}Ca primary beam, provided by the K1200 cyclotron at the National Superconducting Cyclotron Laboratory, in a ^{9}Be production target. The fragments were analyzed using the A1200 fragment separator [18], and the resulting beam was purified by using an aluminum wedge placed in the second dispersive image point of the A1200. The momentum acceptance $\Delta p/p$ of the A1200 was 1%. The ^{42}Ar and ^{44}Ar beams were more than 98% pure with final intensities of 2.7×10^4 and 2.8×10^4 particles per second at the secondary targetand energies of 33.0 and 33.2 MeV/nucleon, respectively.

Two parallel plate avalanche counters [19], placed 82 cm and 183 cm upstream from the secondary target, were used to measure, event by event, the incident beam angle and beam position on the target to correct for the secondary beam emittance. Beam particles were

stopped and identified in a fast/slow phoswich telescope consisting of thin and thick plastic scintillators. This ΔE-E telescope was placed behind the secondary target at 0° so that its opening angle was large enough to detect scattered projectiles with unit efficiency (see Fig. 1). It also yielded a start signal for the proton time-of-flight measurement.

The argon projectiles were scattered by a thin $(CH_2)_n$ target rotated to an angle of 60° with respect to the beam direction, providing an effective in-beam target thickness of 3.12 mg/cm^2, while limiting the energy loss and angular straggling even for low-energy recoiling protons. A group of four telescopes, 5×5 cm^2 active area each, was used to measure the energies and angles of the recoiling protons. Each telescope was composed of a 300 μm thick silicon strip detector with 16 horizontal resistive strips (3 mm wide) backed by two 500 μm thick silicon detectors. The silicon-strip array was positioned 23 cm from the target and covered the laboratory angles between 67° and 82°. A schematic diagram of the experimental setup is shown in Fig. 1.

The telescopes were mounted such that the Si strips were perpendicular to circles of constant scattering angle with respect to the beam line alignment axis. The vertical position was given by the strip which triggered, while the horizontal position was obtained from the charge division signals read out on both ends of the resisitive strips. The horizontal position resolution was about 0.5 mm, corresponding to a resolution of about 0.13° for the in-plane scattering angle. The 3 mm vertical strip pitch corresponds to an angular resolution of about 0.75° for the out-of-plane scattering angle. It should be noted that the larger uncertainty on the vertical position has only a minor affect on the total angular resolution because the detectors are placed rather close to 90° in the laboratory frame, corresponding to small angles in the center-of-mass frame.

Protons that stopped in the silicon strip detector were identified by time-of-flight and energy measurements, while higher energy protons that punched through the first detector were identified by ΔE-E measurements. Protons with energies up to about 14 MeV were stopped in the telescopes. For protons that did not stop in the telescopes, the residual energy was deduced from the energy losses in all three detectors. The final laboratory energy range

was 1–30 MeV, sufficient to detect protons which were elastically scattered and inelastically scattered to the 2_1^+ state in the covered angular range. Proton events in the silicon-strip telescopes were taken in coincidence with the zero degree ΔE-E phoswich detector which identified the outgoing fragments and allowed the scattering channels to be separated from other channels due to reactions with the carbon in the CH_2 target.

Before measuring the ^{42,44}Ar scattering, a test case was run with a ^{36}Ar primary beam degraded to 33.6 MeV/nucleon. Figure 2 shows the excitation spectrum obtained for ^{36}Ar, integrated over the center-of-mass angular range $30° \leq \theta_{cm} \leq 34°$. The first 2^+ excited state of ^{36}Ar located at 1.98 ± 0.06 MeV is clearly identified and its deduced mean energy is in excellent agreement with the adopted value of 1.97 MeV [20]. The excitation energy resolution (FWHM), largely due to the laboratory angle resolution, is of the order of 800 keV.

Figure 3 shows the excitation energy spectra measured for ^{42}Ar and ^{44}Ar. The excitation energy resolution in both cases is similar to that obtained in the ^{36}Ar test case, and the ground state and first 2^+ excited state are clearly identified. The excitation energy of 1.172 ± 0.043 MeV measured for the 2_1^+ state in ^{42}Ar, though slightly smaller, is consistent with the adopted value of 1.208 MeV [20]. The excitation energy of the 2_1^+ state in ^{44}Ar (1.167 ± 0.040 MeV) is in good agreement with the value of 1.144 ± 0.077 MeV obtained in a previous Coulomb excitation measurement [1].

Figure 4 displays the angular distributions for elastic and inelastic scattering to the first 2^+ excited states measured for the ^{36}Ar(p,p') reaction (a), the ^{42}Ar(p,p') reaction (b) and the ^{44}Ar(p,p') reaction (c). These distributions were obtained by fitting the elastic and inelastic peaks, for 1° center-of-mass angular bins, with two Gaussian distributions and then integrating the number of counts. The data were corrected for the geometrical acceptance of the telescopes and an absolute normalization was obtained by using the target thickness and the incident beam intensity given by the 0° phoswich detector. The error bars on Fig. 4 are purely statistical.

III. ANALYSES

A. Phenomenological analysis

Distorded wave Born approximation (DWBA) calculations were performed using the code ECIS [21] and the results are compared to the data in Fig. 4. The optical potential parameters were taken form the Becchetti-Greenlees parametrization [22], which was developed for elastic proton scattering on $A \geq 40$ nuclei. No arbitrary normalization of the data was required and the calculated elastic cross sections, shown by the solid lines in Fig. 4, are directly compared to the absolute experimental cross sections. For the calculation of the inelastic cross sections, a standard vibrational form factor was used, and in each case the quadrupole deformation parameter β_2 was obtained by scaling the calculated inelastic cross section to the data. Similar calculations yielded a good description of the elastic and inelastic proton scattering data for the even-even sulfur isotopes with masses between $A=32$ and $A=40$ [8].

The present analysis yields a value of $\beta_2=0.36$ for the nucleus ^{36}Ar. An experimental uncertainty of $\Delta\beta_2=0.04$ is assigned to this β_2 value based on a visual comparison of the data with the calculations. The range of differential cross sections given by this experimental uncertainty is indicated by the shaded band in Fig. 4. This value of $\beta_2=0.36\pm0.04$ is in excellent agreement with the value obtained from a previous inelastic proton scattering experiment on ^{36}Ar [23]. The same procedure yields values of $\beta_2=0.32\pm0.05$ and 0.31 ± 0.05 for ^{42}Ar and ^{44}Ar, respectively.

It is known that combinations of Coulomb excitation and proton scattering measurements allows one to assess the isoscalar or isovector collective properties of low lying 2^+ and 3^- states [7,24]. The β_2 deformation values extracted here for ^{42}Ar and ^{44}Ar are very close to those measured by Coulomb excitation [1,25], and no clear evidence of an isovector presence in these neutron-rich argon nuclei is seen, contrary to what is observed in the case of the neutron-rich sulfur isotopes [8]. This difference can be explained by the strongly closed

$Z = 16$ sub-shell in sulfur which does not exist for the argon isotopes. In the latter case, the two valence protons can participate to the excitation as much as the neutrons.

B. Microscopic Analysis

In a microscopic model approach to scattering processes, one can view the nucleon-nucleus optical model potential (OMP) as the result of the folding of a complex, energy- and density-dependent effective interaction with the nuclear density. This approach allows for differences in matter densities to be probed because the same nucleon-nucleon effective interaction is used throughout an entire mass chain. In this section, a description of the model and the approximations upon which the calculations are based are presented. The calculations follow the spherical OMP work published in Ref. [26] which was extended to proton inelastic scattering from deformed nuclei in Ref. [8], so only the main features of our approach will be discussed here.

The (p,p') scattering analysis shown below uses deformed OMPs in which point proton and neutron radial densities are calculated through a microscopic collective model for quadrupole motion, as described in Ref. [8,27], using Gogny's Force [28] as an effective interaction. The calculated nuclear densities were then folded with a nucleon-nucleon effective interaction $\mathcal{U}^{JLM}$, which we refer to as the JLM interaction, in order to get the deformed OMPs. Once the diagonal and transition potentials were obtained, they were inserted into the ECIS98 code [21] to solve the coupled equations for proton elastic and inelastic scattering to the first 2^+ excited state of the even-even argon isotopes. Details on the nucleon-nucleon effective interaction as well as on the folding calculations can be found in Ref. [8]. In these calculations, no effective charges and free parameters are introduced. Only small phenomenological renormalizations (λ_v and λ_w) of the real and imaginary potential depths are allowed.

1. Nuclear densities

The point neutron and proton ground state densities as well as the $0^+_{g.s.} \rightarrow 2^+_1$ transition densities calculated with the microscopic collective model are displayed in Fig. 5. The $N = Z$ nucleus ^{36}Ar presents very similar proton and neutron densities as found in ^{32}S, and as expected for light self-conjugate nuclei. For ^{40}Ar, the calculation predicts proton/neutron differences due to the additional neutrons that show up mainly in the interior of the nucleus. Furthermore, both transition densities peak sensibly at the same radius. Moving to the more neutron-rich isotopes, ^{42}Ar and ^{44}Ar, a clear indication of a neutron skin is observed in the ground state densities. A quantitative estimate of this skin can be obtained by comparing the neutron and proton root mean square (rms) radii listed in Table I. Assuming the thickness of the skin is directly given by the difference $\Delta\langle r^2\rangle^{1/2}$ between the neutron and proton rms radii, we find that ^{42}Ar and ^{44}Ar exhibit neutron skins 0.108 fm and 0.147 fm thick, respectively. One should also note that the neutron transition densities for ^{42}Ar and ^{44}Ar are peaked at larger radii than for protons, where the scattering process is most sensitive.

A direct comparison between experimental and calculated charge densities for the ground state of ^{40}Ar is shown on Fig. 6. The experimental charge density was obtained from elastic electron scattering [29]. Although the microscopic calculation does not reproduce the density in the interior of the nucleus, it closely matches the distribution for radii greater than 2.8 fm, where the proton scattering process is most sensitive. This result along with similar ones obtained for the sulfur isotopes [8] sets our optical model calculations on solid ground when using microscopic nuclear densities as described in Refs. [8,27]. Table II lists the experimental 2^+_1 excitation energies and $B(E2, 0^+_{g.s.} \rightarrow 2^+_1)$ values, along with the rms charge radii, and compares them with the theoretical values given by collective Hamiltonian calculations. Except for ^{36}Ar, which will be discussed later, the agreement between the measured and predicted $B(E2)$ values is excellent, showing that the collectivity of these nuclei is well understood. Similar to what was seen in Ref. [8] for the sulfur isotopes, the predicted rms charge radii overestimate the experimental values by 1.5 to 2.5 %.

The ^{36}Ar isotope is a special case since the "standard" collective model calculation that uses the Inglis approximation [30] for the collective mass parameter in the kinetic term of the collective Hamiltonian, predicts prolate $0^+_{g.s.}$ and 2^+_1 states for ^{36}Ar whereas the 2^+_1 state is well known to be oblate [31]. A more complete treatment of the collective mass parameter, using the more self-consistent adiabatic time dependent Hartree-Fock-Bogoliubov (ATDHFB) collective inertia parameters [32], produces an ^{36}Ar nucleus with the expected oblate shape, which manifests itself as the negative sign in the ^{36}Ar transition densities (see Fig. 5). The ATDHFB masses used in this calculation exhibit very sharp peaks in the oblate region of the (β, γ) collective coordinate plane, thus drawing the wave functions towards an oblate deformation. Besides changing the nuclear shape, the collective mass treatment also strongly affects the calculated excitation energy of the first 2^+ state of ^{36}Ar. The energy of this level is predicted to be 2.524 MeV and 1.297 MeV using the Ingliss and ATDHFB collective mass parameters, respectively. The measured excitation energy is 1.970 MeV, between the two collective model predictions, suggesting that the correct treatment of the collective masses lies in between. The calculation using the ATDHFB collective masses strongly underestimates the experimental $B(E2)$ value and thus the collectivity of ^{36}Ar (see Table II). Moreover, the calculated $B(E2)$ values using the Inglis or ATDHFB mass parameters are nearly identical, showing that the collective mass parameters have only a weak influence on the predicted collectivity of ^{36}Ar. Finally, we wish to stress that the ATDHFB approach is not free from approximations, and an even more self-consistent treatment of the collective mass parameters [32] should be performed, presumably with better results.

In Table II, the excitation energies of the first 2^+ states of the ^{40,42,44}Ar isotpes are consistently overestimated by the microscopic collective Hamiltonian calculations (using Inglis collective masses). The above discussion on the effect induced by collective mass parameters suggests that a better treatment of collective masses might improve the agreement.

Finally, the structure calculations for ^{38}Ar are not shown here since they present the same difficulties as those shown in Ref. [8] for ^{36}S, i.e. the collectivity of these $N=20$ nuclei is strongly overestimated by the microscopic collective Hamiltonian predictions. One

can nevertheless notice that the $B(E2) = 129 \pm 10$ e^{2}fm^4 experimental value for ^{38}Ar [25] is the lowest one among the argon isotopes, which is consistent with the presence of the $N = 20$ shell closure. This low $B(E2)$ value is due to the vanishing of the neutron pairing for spherical shapes.

Model-dependent quadrupole deformation parameters were calculated from microscopic predictions using

$$\beta_2^{n(p)} = \frac{\sqrt{5\pi}\, Q_2^{n(p)}}{3\, N(Z)\, R^2} \tag{1}$$

where $Q_2^{n(p)}$ is the neutron (proton) quadrupole moment, R the nucleus radius defined as $r_0\, A^{1/3}$ ($r_0 = 1.2$ fm), and $N(Z)$ is the neutron (proton) number. The deformation parameters for the neutron, proton, and matter distributions are listed in Table III. The isotopes ^{40,42,44}Ar all exhibit neutron quadrupole deformations that are significantly larger than the ones for protons, which is consistent with the observation that the neutron transition densities peak at larger radii than the proton densities (see Fig. 5). This difference is also reflected in the M_n/M_p ratios which increase with the neutron richness as in Ref. [8] in the case of sulfur isotopes. Predicted values for the matter deformation can also be compared with the phenomenological values extracted from the DWBA analysis. Both values are very close and exhibit the same increasing trend with heavier masses. In the case of ^{36}Ar, the proton and neutron deformations are nearly identical as expected for a light $N = Z$ nucleus. Also the underestimation of the $B(E2)$ value for this nucleus translates into an underestimation of the β_2 deformation parameter, which is predicted to be of the order of $\beta_2 = -0.20$ whereas the DWBA analysis finds $|\beta_2| = 0.36 \pm 0.04$. In summary, moving along the argon isotopic chain, the matter deformation changes from strongly oblate for ^{36}Ar to more prolate for ^{40,42,44}Ar, with a nearly spherical shape for ^{38}Ar.

2. Microscopic optical model calculations

The microscopic calculations are compared in Fig. 7 with experimental elastic and inelastic scattering angular distributions for several argon isotopes, with the exception of ^{38}Ar

for which no experimental proton scattering data are available. For all argon isotopes studied here the λ_v and λ_w potential depth normalization factors where taken to be 0.94 and 0.92, respectively. As in Ref. [8], the isovector parts of the nuclear central potential were multiplied by 2.0 in order to be able to use the same λ parameters throughout the argon isotopic chain. A remarkable agreement is observed both in shape and magnitude for all argon isotopes but for ^{36}Ar. The first diffraction minima and maxima for the elastic and inelastic scattering are well reproduced. Note that the small overestimation of the charge rms radii discussed above does not seem to adversely affect either the position or the depth of the predicted diffraction minima. Similarly, the small differences between the phenomenological quadrupole deformations and those obtained from the microscopic collective model are not evident from the inspection of the calculated inelastic scattering cross sections shown in Fig. 7.

In the case of ^{36}Ar, the calculation that uses the densities calculated with the microscopic collective Hamiltonian and the ATDHFB mass parameters, underpredicts the inelastic scattering cross section by about a factor of 2 (solid line in Fig. 7). This underestimation of the collectivity of ^{36}Ar (by the collective Hamiltonian calculations) can be expected from the comparison between the predicted and measured $B(E2, 0^+_{g.s.} \rightarrow 2^+_1)$ values (see Sec. III B 1). A calculation performed using axial Hartree-Fock-Bogoliubov densities constrained at $\beta = -0.30$ (dotted line in Fig. 7) yields much better results and agrees with the $|\beta_2|$ value extracted from the DWBA analysis using phenomenological optical potentials.

Overall, the good agreement between the calculated and experimental cross section angular distributions shows that the JLM interaction, folded with our microscopic densities to produce a microscopic OMP, is a reliable tool for analyzing proton scattering data for stable and unstable nuclei in the argon region, which is consistent with the conclusions of Ref. [8]. The case of ^{36}Ar shows that (p,p') scattering calculations using our folding OMP are very sensitive to the collectivity of the folded nuclear density, and thus can be used as tests for different descriptions of nuclear structure.

IV. SUMMARY AND CONCLUSIONS

In summary, we have measured the cross section angular distributions for elastic and inelastic scattering of protons on the unstable neutron-rich nuclei ^{42}Ar and ^{44}Ar. The experiment was performed in inverse kinematics using secondary radioactive beams and detection of the recoiling protons. This measurement extends the systematics of proton scattering from the even-even argon isotopes. These results combined with those already obtained for the sulfur isotopic chain provide a unique opportunity to study the collective properties of nuclei in the $A = 40$ mass region moving through the $N = 20$ shell closure towards the neutron-rich side of the valley of stability.

The data were first analyzed in the framework of a phenomenological optical model using the Becchetti-Greenlees parametrization and standard collective transition form factors. The calculations were in excellent agreement with the experimental angular distributions, and β_2 values of 0.32 ± 0.05 and 0.31 ± 0.05 were extracted for ^{42}Ar and ^{44}Ar, respectively. These deformation values are very close to those measured by Coulomb excitation, and no clear evidence of isovector behavior in the neutron-rich nuclei ^{42}Ar and ^{44}Ar is observed.

Microscopic OMP calculations were also performed for the argon isotopes. These calculations consisted of folding a modified JLM effective interaction with nuclear densities obtained by solving the collective Hamiltonian for quadrupole motion. The deformed microscopic OMPs were then used to solve the coupled equations for elastic and inelastic proton scattering by the 0^+ ground states and 2_1^+ excited states of the even-even argon isotopes. For the isotopes ^{40,42,44}Ar, this microscopic approach produces predictions that agree very well with the experimental (p,p') data. This can be interpreted as the fact that i) the reaction model, ii) the folding model, iii) the modified JLM effective interaction (including a sizable renormalization of the isovector part), and iv) the description of nuclear structure in terms of the collective model, are providing adequate representations of the physics involved in (p,p') scattering from these isotopes. Moreover, the deformation parameters deduced from the microscopic structure calculations confirm those inferred from our phenomenological analysis.

However, the above calculation scheme does not account for (p,p') scattering on ^{36}Ar. The obvious cause of this disagreement is the underprediction of the collectivity of ^{36}Ar by the microscopic collective models. Yet, given a more deformed nuclear density, the microscopic OMP predictions agree with both experimental (p,p') data and their phenomenological interpretation. This shows that our microscopic OMP can be viewed as a direct link between experimental proton scattering data and nuclear structure calculations, and constitutes a powerful tool to test densities obtained from various descriptions of nuclear structure.

This work was partly supported by the National Science Foundation under contracts PHY-9528844, PHY-9602927, PHY-9523974 and PHY-9605207.

REFERENCES

* Present address: Max Plank Insitut für Kernphysik, 69029 Heidelberg, Germany.

[1] H. Scheit, T. Glasmacher, B.A. Brown, J.A. Brown, P.D. Cottle, P.G. Hansen, R. Harkewicz, M. Hellstrom, R.W. Ibbotson, J.K. Jewell, K.W. Kemper, D.J. Morrissey, M. Steiner, P. Thirolf, and M. Thoennessen, Phys. Rev. Lett. **77**, 3967 (1996).

[2] T. Glasmacher, B.A. Brown, M.J. Chromik, P.D. Cottle, M. Fauerbach, R.W. Ibbotson, K.W. Kemper, D.J. Morrissey, H. Scheit, D.W. Sklenicka, and M. Steiner, Phys. Lett. B **395B**, 163 (1997).

[3] R.W. Ibbotson, T. Glasmacher, B.A. Brown, L. Chen, M.J. Chromik, P.D. Cottle, M. Fauerbach, K.W. Kemper, D.J. Morrissey, H. Scheit, and M. Thoennessen, Phys. Rev. Lett. **80**, 2081 (1998).

[4] T.R. Werner, J.A. Sheikh, W. Nazarewicz, M.R. Strayer, A.S. Umar, and M. Misu, Phys. Lett. **333B**, 303 (1994).

[5] T.R. Werner, J.A. Sheikh, M. Misu, W. Nazarewicz, J. Rikovska, K. Heeger, A.S. Umar, and M.R. Strayer, Nucl. Phys. **A597**, 327 (1996).

[6] J. Retamosa, E. Caurier, F. Nowacki, and A. Poves, Phys. Rev. C **55**, 1266 (1997).

[7] J.H. Kelley, T. Suomijärvi, S.E. Hirzebruch, A. Azhari, D. Bazin, Y. Blumenfeld, J.A. Brown, P.D. Cottle, S. Danczyk, M. Fauerbach, T. Glasmacher, J.K Jewell, K.W. Kemper, F. Maréchal, D.J. Morrissey, S. Ottini, J.A. Scarpaci, and P. Thirolf, Phys. Rev. C **56**, R1206 (1997).

[8] F. Maréchal, T. Suomijärvi, Y. Blumenfeld, A. Azhari, E. Bauge, D. Bazin, J.A. Brown, P.D. Cottle, J.P. Delaroche, M. Fauerbach, M. Girod, T. Glasmacher, S.E. Hirzebruch, J.K. Jewell, J.H. Kelley, K.W. Kemper, P.F. Mantica, D.J. Morrissey, L.A. Riley, J.A. Scarpaci, H. Scheit, and M. Steiner, Phys. Rev. **C60**, 034615 (1999).

[9] A.M. Bernstein, V.R. Brown, and V.A. Madsen, Phys. Lett. **103B**, 255 (1981).

[10] G. Kraus, P. Egelhof, C. Fischer, H. Geissel, A. Himmler, F. Nickel, G. Munzenberg, W. Schwab, A. Weiss, J. Friesse, A. Gillitzer, H.J. Korner, M. Peter, W.F. Henning, J.P. Schiffer, J.V. Kratz, L. Chulkov, M. Golovkov, A. Ogloblin, and B.A. Brown, Phys. Rev. Lett **73**, 1773 (1994).

[11] A.A. Korsheninnikov, E.A. Kuzmin, E.Yu. Nikolsky, O.V. Bochkarev, S. Fukuda, S.A. Goncharov, S. Ito, T. Kobayashi, S. Momota, B.G. Novatsky, A.A. Ogloblin, A. Ozawa, V. Pribora, I. Tanihata, and K. Yoshida, Phys. Rev. Lett. **78**, 2317 (1997).

[12] L.A. Riley, J.K. Jewell, P.D. Cottle, T. Glasmacher, K.W. Kemper, N. Alamanos, Y. Blumenfeld, J.A. Carr, M.J. Chromik, R.W. Ibbotson, F. Maréchal, W.E. Ormand, F. Petrovich, H. Scheit, and T. Suomijärvi, Phys. Rev. Lett. **82**, 4196 (1999).

[13] J.K. Jewell, L.A. Riley, P.D. Cottle, K.W. Kemper, T. Glasmacher, R.W. Ibbotson, H. Scheit, M.J. Chromik, Y. Blumenfeld, S.E. Hirzebruch, F. Maréchal, and T. Suomijärvi, Phys. Lett. **B454**, 181 (1999).

[14] F. Maréchal, T. Suomijärvi, Y. Blumenfeld, A. Azhari, D. Bazin, J.A. Brown, P.D. Cottle, M. Fauerbach, T. Glasmacher, S.E. Hirzebruch, J.K. Jewell, J.H. Kelley, K.W. Kemper, P.F. Mantica, D.J. Morrissey, L.A. Riley, J.A. Scarpaci, H. Scheit, and M. Steiner, Phys. Rev. **C60**, 064623 (1999).

[15] J.J. Kelly, M.A. Khandaker, P. Boberg, A.E. Feldman, B.S. Flanders, S. Hyman, H. Seifert, P. Karen, B.E. Norum, P. Welch, S. Nanda, and A. Saha, Phys. Rev. C **44**, 1963 (1991).

[16] M.A. Khandakar, J.J. Kelly, P. Boberg, A.E. Feldman, B.S. Flanders, S. Hyman, H. Siefert, P. Karen, B.E. Norum, P. Welch, S. Nanda, and A.Saha, Phys. Rev. C **44**, 1978 (1991).

[17] A.E. Feldman, J.J. Kelly, B.S. Flanders, M.A. Khandakar, H. Siefert, P. Boberg, S.D.

Hyman, P.H. Karen, B.E. Norum, P. Welch, Q. Chen, A.D. Bacher, G.P.A. Berg, E.J. Stephenson, S. Nanda, A. Saha, and A. Scott, Phys. Rev. C **49**, 2068 (1994).

[18] B.M. Sherrill, D.J. Morrissey, J.A. Nolen, Jr., N. Orr, and J.A. Winger, Nucl. Instrum. Methods Phys. Res. **B70**, 298 (1992).

[19] D. Swan, J. Yurkon, and D. Morrissey, Nucl. Instrum. Methods Phys. Res. **A348**, 314 (1994).

[20] P.M. Endt, Nucl. Phys. A521, 1 (1990).

[21] J. Raynal, Phys. Rev. C **23**, 2571 (1981). J. Raynal, CEA report No CEA-N-2772, 1994.

[22] F.D. Becchetti, Jr., and G.W. Greenlees, Phys. Rev. **182**, 1190 (1969).

[23] R.R. Johnson, and R.J. Griffiths, Nucl. Phys. **A117**, 273 (1968).

[24] A.M. Bernstein, V.R. Brown, and V.A. Masden, Comments Nucl. Part. Phys. **11**, 203 (1983).

[25] S. Raman, C.H. Malarkey, W.T. Milner, C.W. Nestor, Jr., and P.H. Stelson, Atomic Data and Nuclear Data Tables **36**, 1 (1987).

[26] E. Bauge, J.P. Delaroche, and M. Girod, Phys. Rev. C **58**, 1118 (1998).

[27] J. Libert, M. Girod, J.P. Delaroche, Phys. Rev. C **60**, 054301 (1999).

[28] J.F. Berger, M. Girod, and D. Gogny, Comput. Phys. Commun. **63**,365 (1990). J. Dechargé, and D. Gogny, Phys. Rev. C **21**, 1568 (1980).

[29] C.R. Ottermann, Ch. Schmitt, G.G. Simon, F. Borkowski, and V.H. Walther, Nucl. Phys. **A379**, 396 (1982).

[30] D.R. Inglis, Phys. Rev. **103**, 1786 (1956); S.T. Belayev, Nucl. Phys. **24**, 322 (1961).

[31] P. Raghavan, At. Data Nucl. Data Tables, **42**, 189 (1989).

[32] E.Kh. Yuldashbaeva, J. Libert, P. Quentin, and M. Girod, Phys. Lett. **461B**, 1 (1999).

[33] J.M. Finn, H. Crannell, P.L. Hallowell, J.T. O'Brien, and S. Penner, Nucl. Phys. **A274**, 28 (1976).

[34] R. DE Leo, S. Micheletti, M. Pignanelli, and M.N. Harakeh, Phys. Rev. C **31**, 362 (1985).

FIGURES

FIG. 1. Schematic diagram of the experimental setup. Four silicon-strip telescopes that detected recoiling protons from a CH_2 target were placed on each side of the beam direction. A cylindricalplastic phoswich detector was placed at 0° and measured both incident beam and scattered fragments. Two parallel plate avalanche counters placed before the target were used to track the beam event by event.

FIG. 2. Excitation energy spectrum for ^{36}Ar scattering on protons at 33.6 MeV/nucleon integrated over the center-of-mass angular range $30° \leq \theta_{cm} \leq 34°$. The solid line is the sum of Gaussian fits to the elastic and inelastic peaks.

FIG. 3. Excitation energy spectra for ^{42}Ar and ^{44}Ar integrated over the 29°-37° and 27°-33° center-of-mass angular bins,respectively. The dark and light grey areas are Gaussian fits to the elastic and inelastic peaks. The solid line is the sum of the two contributions. The center-of-mass angular range and measured excitation energy of the first 2^+ excited state are listed for both nuclei.

FIG. 4. Angular distributions for the elastic scattering (open circles) and inelastic scattering to the first 2^+ excited state (filled circles) measured for (a) the ^{36}Ar(p,p') reaction at 33.6 MeV/nucleon, (b) the ^{42}Ar(p,p') reaction at 33.0 MeV/nucleon, and (c) the ^{44}Ar(p,p') reaction at 33.2 MeV/nucleon. DWBA calculations using the Becchetti-Greenlees optical potential are shown for the ground state (solid line) and for the 2^+ state (dashed line) (see text). The shaded bands indicate the experimental uncertainty for the deformation parameter β_2.

FIG. 5. Microscopic collective model predictions for the ground state (top row) and transition densities to the 2_1^+ state (bottom row) for even-even argon isotopes ranging from ^{36}Ar to ^{44}Ar. The solid lines represent the proton densities whereas the dashed lines are the neutron densities. The ^{36}Ar densities are calculated using the ATDHFB collective mass parameters (see text).

FIG. 6. Comparison between experimental (solid line) and predicted (dashed line) monopole charge density for ^{40}Ar. Experimental data are extracted from Ref. [29]. The predicted charge density is obtained by convoluting the calculated proton density with the proton charge smearing form factor.

FIG. 7. Microscopic coupled channel calculations using microscopic collective model densities and the JLM nucleon-nucleon interaction for the ground state (solid line) and the 2_1^+ state (dashed line) (see text). The experimental data are from the present work (^{36,42,44}Ar) and from Ref. [34] (^{40}Ar at 35.1 MeV). A calculation using axial HFB densities constrained at $\beta = -0.30$ is also shown for ^{36}Ar (dotted line).

TABLES

TABLE I. Proton and neutron root mean square (rms) radii calculated using the microscopic collective model described in the text.

	r^p_{rms} (fm)	r^n_{rms} (fm)	$\Delta\langle r^2\rangle^{1/2}$ (fm)
^{36}Ar	3.331	3.285	-0.045
^{40}Ar	3.377	3.441	0.064
^{42}Ar	3.400	3.508	0.108
^{44}Ar	3.419	3.566	0.147

TABLE II. Energies of the 2^+_1 state, $B(E2)$ values and rms charge radii. Experimental excitation energy and $B(E2)$ values are from Ref. [25] ($^{36-42}$Ar) and from Ref. [1] (^{44}Ar). Experimental rms charge radii are from Ref. [33] (^{36,40}Ar). Theoretical values are from the microscopic collective model calculations using the ATDHFB (^{36}Ar) and Inglis ($^{40-44}$Ar) collective masses.

	$E^*_{2^+}$ (MeV)		$B(E2)$ (e^2fm^4)		r^c_{rms} (fm)	
	exp.	theory	exp.	theory	exp.	theory
^{36}Ar	1.970	1.297	340 ± 40	191.67	3.327 ± 0.015	3.393
^{40}Ar	1.461	2.528	330 ± 39	280.01	3.393 ± 0.015	3.432
^{42}Ar	1.208	2.024	420 ± 100	344.00	-	3.453
^{44}Ar	1.144	1.603	345 ± 41	375.81	-	3.469

TABLE III. Matter, proton and neutron deformations and M_n/M_p ratios from the microscopic collective model calculations.

	β_2^m	β_2^p	β_2^n	$(M_n/M_p)/(N/Z)$
^{36}Ar	-0.203	-0.205	-0.200	0.976
^{40}Ar	0.233	0.225	0.240	1.064
^{42}Ar	0.263	0.244	0.278	1.137
^{44}Ar	0.271	0.247	0.288	1.169